A novel role for Cyclic Nucleotide-Gated Ion Channel 2 (DND1) in auxin signaling

Sonhita Chakraborty[1], Masatsugu Toyota[2], Wolfgang Moeder[1], Kimberley Chin[1], Alex Fortuna[1], Marc Champigny[3*], Steffen Vanneste[4,5], Simon Gilroy[6], Tom Beeckman[4,5], Keiko Yoshioka[1,7]

[1] Department of Cell and Systems Biology, University of Toronto, 25 Willcocks Street, Toronto, ON, M5S 3B2, Canada

[2] Department of Biochemistry and Molecular Biology, Saitama University, 255 Shimo-Okubo, Sakura-ku, Saitama, 338-8570, Japan

[3] Department of Biology, McMaster University, Hamilton, ON, L85 4K1, Canada

[4] Department of Plant Biotechnology and Bioinformatics, Ghent University, 9052 Ghent, Belgium

[5] VIB Center for Plant Systems Biology, 9050 Gent, Belgium

[6] Department of Botany, University of Wisconsin, Madison, 53706, USA

[7] Center for the Analysis of Genome Evolution and Function (CAGEF), University of Toronto, 25 Willcocks Street, Toronto, ON, M5S 3B2, Canada

*Current position: PhenoLogic Co., Toronto, ON, M5A 2N1, Canada

ABSTRACT

Cyclic Nucleotide Gated Ion Channels (CNGCs) are non-selective cation channels that are involved in regulating responses to both biotic and abiotic stresses in plants. CNGC2 has been implicated in plant immunity and Ca^{2+} signaling through the study of the autoimmune phenotypes exhibited by the null mutant, *defense, no death1* (*dnd1*). However, *dnd1* also shows additional phenotypes that are unique among autoimmune mutants. This suggests that CNGC2 plays multiple biological roles beyond pathogen defense. In this study, we cloned the gene that encodes the first suppressor of *dnd1 (cngc2)*, *REPRESSOR OF DEFENSE, NO DEATH1* (*RDD1),* which encodes an auxin biosynthesis gene, *YUCCA6* (*YUC6*). We found that *dnd1 (cngc2)* is defective in auxin-mediated root growth inhibition and gravitropic responses in roots. Consistently with these auxin resistance phenotypes, we found *dnd1* shows a dampened response to exogenous auxin compared to wildtype plants using the auxin inducible DR5::GUS and DII:VENUS reporter systems. Finally, auxin-induced Ca^{2+} influx was examined using the Förster resonance energy transfer (FRET)-based, genetically encoded Ca^{2+} indicator yellow cameleon (YC)-Nano65. We captured severe defects in auxin-induced Ca^{2+} increase in *dnd1*. These defects were rescued by the *rdd1* mutation. Our findings highlight the unexpected involvement of CNGC2 in auxin-induced Ca^{2+} signaling and calls into question the current interpretation of *dnd1* phenotypes in defense signaling.

INTRODUCTION

Calcium (Ca^{2+}) is a ubiquitous secondary messenger that orchestrates many signaling pathways in all eukaryotes [1]. Indeed, transient changes in cytosolic free Ca^{2+} concentrations ($[Ca^{2+}]_{cyt}$) are elicited in plants by a diverse range of abiotic stresses such as drought, heat, wounding; biotic stimuli in the form of interactions with pathogenic and symbiotic microorganisms, as well as in response to developmental cues [2,3]. The perception of different stimuli generates specific spatio-temporal "Ca^{2+} signatures" which are decoded by the direct binding of Ca^{2+} to Ca^{2+} sensor proteins such as calmodulins (CaM), Calcium dependent protein kinases (CDPK), etc [4]. These sensor proteins may undergo conformational changes upon binding and interact with or phosphorylate various target substrates to regulate their downstream function [4,5]. The Ca^{2+} flux that is essential for the generation of these Ca^{2+} signatures is regulated by a combination of various channels, pumps and transporters, which translocate Ca^{2+} between extracellular and/or intracellular Ca^{2+} stores to the cytoplasm. Despite the central role for Ca^{2+}, the identity of plant Ca^{2+} channels that regulate $[Ca^{2+}]_{cyt}$ to most stimuli still remains elusive [3 -7].

Cyclic nucleotide gated ion channels (CNGCs) are nonselective cation channels that have been reported to function as Ca^{2+} channels or are associated with Ca^{2+} signaling in plants [8–11]. Plant CNGCs are involved in a wide variety of physiological processes that are known to be regulated by Ca^{2+} signaling, such as pollen tube growth, pollen-pistil interaction, thermo-sensing, pathogen resistance and symbiotic interactions [11–13]. The involvement of CNGCs in plant defense was first suggested through the study of the Arabidopsis null mutant *of CNGC2*, *defense, no death1* (*dnd1*). *dnd1* shows autoimmune phenotypes including stunted morphology, conditional spontaneous cell death and elevated basal levels of salicylic acid (SA), that confer enhanced resistance against various pathogens [14,15]. Initially, *dnd1* was discovered for its reduced ability to mount a hypersensitive response (HR), which is a form of programmed cell death (PCD) around the site of pathogen infection and a hallmark of effector triggered immunity [15]. Later two *CNGC4* null mutants, *HR-like lesion mimic 1 (hlm1)*[16] and *defense, no death2*

(*dnd2*)[17], and *cpr22,* a gain-of-function mutant of *CNGC12,* were also found to be involved in defense [18]. The inhibition of *cpr22*-mediated PCD by Ca^{2+} channel blockers, and the higher $[Ca^{2+}]_{cyt}$ levels in *cpr22* further support the notion that *CNGC12* is a positive regulator of plant defense by activating Ca^{2+} signals [3,12,19]. On the other hand, the reduced HR phenotype and suppression of Ca^{2+} signals upon pathogen elicitors in *dnd1* suggest that CNGC2 is also a positive regulator of defense [20]. However, the autoimmunity phenotype of *dnd1* contradicts this notion [12].

dnd1 is hypersensitive to elevated Ca^{2+} [21]. A microarray study revealed that the gene expression pattern of *dnd1* plants resembles that of wildtype plants under elevated Ca^{2+} stress [22]. Recent work further implicates CNGC2 in maintaining Ca^{2+} homeostasis by facilitating Ca^{2+} unloading from the vasculature and influx into leaf cells[23]. Interestingly, the Ca^{2+} hypersensitivity of *dnd1* is likely also the cause of the autoimmune phenotypes (high SA levels, H_2O_2 accumulation and cell death) associated with this mutant since these phenotypes are largely lacking when *dnd1* seedlings are grown in media with low Ca^{2+} [22].

In addition, *dnd1* is also tolerant to heat stress and exhibits higher and/or earlier accumulation of heat shock proteins [24,25]. *dnd1* also displays delayed flowering time, this is uncharacteristic for SA-accumulating autoimmune mutants, which usually exhibit early flowering phenotypes [26,27]. CNGC2-mediated Ca^{2+} signaling also has been suggested to be important in CLAVATA3/CLAVATA1 (CLV3/CLV1) signaling in determining shoot apical meristem (SAM) size [28]. Collectivity, these observations illustrate possible roles of CNGC2 beyond pathogen defence.

In order to study CNGC2 (DND1)-mediated signal transduction, we conducted a suppressor screen of a *cngc2* null mutant and identified the first *dnd1* suppressor mutant named *repressor of defense, no death1* (*rdd1-1 cngc2*) [26]. The *rdd1-1* mutation can supress almost all *dnd1*-related phenotypes except its Ca^{2+} hypersensitivity, indicating that *RDD1* is involved

downstream of CNGC2's channel function. In this work, we have identified the causal mutation of *rdd1-1* as a point mutation in the auxin biosynthesis gene YUCCA6 (YUC6). We discovered that *cngc2* has a defect in auxin responses and this is likely due to the alteration of Ca^{2+} signals upon auxin sensing, revealing an exciting novel role of CNGC2 in auxin signaling.

RESULTS

RDD1 encodes YUCCA6

To clone RDD1, *rdd1-1 cngc2-3* (a CNGC2 T-DNA insertion line that is identical to *dnd1*, which is a premature stop codon null mutant, Columbia ecotype background) plants were outcrossed to *cngc2-1* (Ws ecotype background) to generate a mapping population. Using 705 plants of this F2 mapping population, the RDD1 locus was mapped to an approximate 800kb region that contains 193 coding sequences [26]. Through whole genome sequencing, the causative mutation of *rdd1-1* was narrowed down to four putative candidate genes within this region: *AT5G24680*, *AT5G25590*, *AT5G25620* or *AT5G26050*. Of these mutations, only the mutation in *AT5G25620* was located in a coding region, more specifically, within the second exon. q-RT PCR analysis revealed that *rdd1-1* does not have significant alterations in the expression of the three other candidate genes (data not shown**)**. Thus, the causative mutation is likely a non-synonymous amino acid change from proline to leucine at residue 289 in AT5G24620, which encodes the protein YUC6, a flavin-containing monooxygenase-like (FMO) protein involved in a key step in auxin biosynthesis [29,30].

rdd1-1 is a loss-of-function allele of YUC6

Given that *rdd1* is a point mutation that does not cause a premature stop codon or frame shift in the YUC6 gene, the phenotype of its suppression of *dnd1* would most likely be associated with either a gain or loss-of-function of this enzyme. To test which of these alternatives was likely in operation, we tested if either *yuc6-1D*, a YUC6 overexpressing activation mutant [31] or *yucca6-3k*

(henceforth, *yuc6*), a YUC6 knockout mutant [32], can suppress *dnd1* phenotypes. *yuc6-1D* was unable to suppress *dnd1* as none of the 132 plants analyzed in the F2 generation of the cross between *yuc6-1D* and *cngc2* displayed a *rdd1-1 cngc2-like* rescue of the *cngc2* dwarf morphology. Besides the expected *cngc2* dwarf phenotype and typical auxin over-accumulating phenotype of *yuc6-1D* (e.g., long narrow leaves with elongated petioles[31]), we observed an additional phenotype with *yuc6-1D*-like leaf shape but significantly smaller stature than *yuc6-1D,* similarly to the size difference between *cngc2* and WT from these crosses **(Supplemental Figure S1)**. Genotyping identified these smaller *yuc6-1D* looking plants as having a *cngc2* homozygous background. Our genetic analysis therefore shows that *yuc6-1D* does not suppress the small rosette phenotype of *cngc2* and double homozygous plants display both a *yuc6-1D* phenotype and *cngc2*-like smaller statue **(Supplemental Table S1).** On the other hand, the loss-of-function mutant *yuc6* was able to suppress the *dnd1* phenotype. The phenotypes of *yuc6 cngc2* and *rdd1-1 cngc2* found in the F2 population of the cross between *yuc6* and *cngc2* were identical **(Figure 1A upper panel)**. In addition, we noticed that *rdd1-1* single mutants showed the same broad leaf phenotype of *yuc6,* further supporting the notion that *rdd1-1* is a loss-of-function allele of *YUC6* **(Supplemental Figure S2)**. However, unexpectedly, the number of *cngc2*-like plants in this F2 population was more than the predicted number based on the assumption that *rdd1-1* (therefore also *yuc6)* is dominant in terms of suppression of *cngc2* [26]. Moreover, the variation of phenotypes was highly environmentally sensitive, making it difficult to acquire conclusive segregation data in this F2 population. Thus, we conducted alternative genetic analyses with B2 populations of a backcross of *yuc6 cngc2* x *cngc2*. Careful phenotyping revealed a 1:2:1 segregation with 50% of the plants exhibiting an intermediate phenotype **(Supplemental Table S2** and **Supplemental Figure S3)**, indicating semi-dominance or a dosage effect of *yuc6* to supress *cngc2*. Originally, *rdd1-1* was described as a dominant mutant based on morphological segregation [26]. Therefore, this data was unexpected (the predicted dominant phenotype should have segregated with a 3:1 ratio of

rescued:*cngc2* dwarf phenotypes). Thus, we conducted a similar analysis using B2 populations of a backcross of *rdd1-1 cngc2* x *cngc2*. Strikingly, it showed the same 1:2:1 segregation with 50% of the plants exhibiting an intermediate phenotype, just like the B2 populations of *yuc6 cngc2* **(Supplemental Table S3** and **Supplemental Figure S3)**. The difference from the previously published analysis [26] of the *rdd1-1* segregation analysis can probably be explained by the environmental sensitivity of the penetrance of *cngc2*. Taken together, we concluded that *rdd1-1* is a loss-of-function mutant of *YUC6* and it is semi-dominant (having a dosage effect) in terms of suppression of *cngc2*.

To further validate the suppression of *dnd1*-mediated phenotypes by a loss-of-function of YUC6, the *yuc6 cngc2* double mutant was analyzed in detail. *dnd1* displays conditional spontaneous cell death formation which is suppressed by *rdd1-1* [26]. As observed by the trypan blue staining of 4-week old plants, *yuc6 cngc2* also displayed less spontaneous cell death than *cngc2* **(Figure 1A, lower panel).** *dnd1* (*cngc2*) shows enhanced resistance to various pathogens such as the bacterial pathogen, *Pseudomonas syringae* pv. t*omato* (*Pst*), and the oomycete pathogen, *Hyalopernospora arabidopsidis* (*Hpa*) [14,15] and this enhancement is suppressed in *rdd1-1 cngc2* [26]. A breakdown of the enhanced pathogen resistance of *dnd1* (*cngc2*) to *Hpa,* isolate Noco2, was also observed in *yuc6 cngc2* **(Figure 1B** and **C)**, similar to *rdd1-1 cngc2* [26]**.** This also was mirrored by a reduction of SA levels to the same degree in *yuc6 cngc2* as in *rdd1-1 cngc2* **(Figure 1D).** Furthermore, *dnd1* exhibits delayed flowering. This phenotype is also suppressed in *rdd1-1 cngc2* and has since been shown to not rely on SA-dependent signaling mechanisms [27]. Like *rdd1-1 cngc2, yuc6 cngc2* showed not only suppression of the delayed flowering phenotype, but instead a premature flowering phenotype compared to Col-wt and the *yuc6* single mutant **(Figure 1E)**. Taken together, we concluded that *cngc2* phenotypes can be suppressed by a loss-of-function mutation in *YUC6*.

dnd1 (cngc2) has alterations in auxin-mediated phenotypes that are rescued in *rdd1-1 cngc2*

dnd1 (*cngc2*) exhibits characteristics that are not typical of a lesion mimic mutant (LMM) such as delayed flowering and Ca^{2+} hypersensitivity [21,27,33]. Given that *RDD1* encodes the auxin biosynthesis gene *YUC6*, we hypothesized that CNGC2 may also be involved in auxin signalling. Thus, we re-characterized *dnd1 (cngc2)* to examine if it displayed alterations in auxin sensitivity and/or response. As a first readout of auxin response, we analyzed the root gravitropic response of the mutant [34,35]. As shown in **Figure 2A**, *dnd1* (*cngc2*) exhibited a delayed gravitropic root tip bending response, which was partially recovered in *rdd1-1 cngc2*. Auxin inhibits root growth elongation at low concentrations [36], thus represents an easy readout for evaluating auxin sensitivity [37,38]. As shown in **Figure 2B** and **2C**, addition of 0.1µM IAA or the synthetic auxin, NAA, supressed root growth in Col-wt, showing 64% and 54% of control root length, respectively. However, in *cngc2* this root growth inhibition was much less pronounced, consistent with a reduced auxin sensitivity **(Figure 2B** and **C)**. Interestingly, this auxin insensitivity in *cngc2* was also supressed by the *rdd1-1* mutation **(Figure 2B** and **C)**. Collectively, these data suggest that *dnd1 (cngc2)* has alterations in auxin sensitivity and/or signaling and the *rdd1-1* mutation can rescue this phenotype similar to most other *dnd1 (cngc2)* phenotypes.

dnd1 (cngc2) plants display impaired auxin signaling

The delayed gravitropic response and reduced auxin sensitivity of root growth in *dnd1* led us to analyze the auxin responsiveness of the canonical auxin signaling pathway in *dnd1* using the well-established artificial auxin response reporter DR5 fused to GUS (DR5::GUS), as well as the Aux/IAA-based auxin signaling sensor DII:VENUS [39,40]. The GUS activity was significantly lower in the root and shoots of *cngc2* relative to those of Col-wt 24 hours after treatment of 1µM IAA (**Figure 3A**). This indicates that the transcriptional auxin response is

impaired in *cngc2*. A partial recovery of this impairment was observed in *rdd1-1 cngc2* shoots and a complete recovery was noted in *rdd1-1 cngc2* roots. To support these observations, we analyzed transcriptional induction of the auxin-inducible gene *IAA1* upon exogenous auxin treatment. A significant induction of *IAA1* was observed in Col-wt, however no induction was seen in *cngc2* 24 hours after treatment with1µM IAA. As expected, *rdd1-1 cncg2* displayed a partial rescue **(Figure 3B)**.

Next, we analyzed the auxin responsiveness of the Aux/IAA degradation sensor DII-VENUS in these mutants. As expected, after the addition of 1µM IAA to root tips a rapid decay in VENUS signal was observed over a 20 minute time period in 5-day old DII:VENUS Col-wt seedlings. Corroborating our DR5::GUS data, the auxin-induced decay of DII-VENUS signal was slower and dampened in DII:VENUS *cngc2* and this was partially rescued in the DII:VENUS *rdd1-1 cngc2* roots **(Figure 3C)**. Taken together, these data strongly suggest *CNGC2* is involved in early auxin signaling.

CNGC2 is involved in auxin induced Ca^{2+} signals

It has been previously shown that exogenous auxin can induce a Ca^{2+} influx in processes such as gravitropism [41–44]. Thus, it is plausible that the defective auxin-mediated responses of *dnd1* are due to the alterations in CNGC2-generated Ca^{2+} signals ($[Ca^{2+}]_{cyt}$ increase). In other words, CNGC2 might be involved in auxin-induced Ca^{2+} signal activation. To investigate this point, we analyzed Col-wt, *dnd1* and *rdd1-1 cngc2* (*rdd1-1 dnd1* equivalent, Note: Due to the antibiotic resistance gene, we had to use *dnd1* instead of *cngc2*) carrying the FRET-based Ca^{2+} sensor Yellow Chameleon (YC)-Nano65 [45]. Auxin treatment at the top area rapidly induced a clear increase in $[Ca^{2+}]_{cyt}$ in Col- wt (Region of interest 1, ROI1, **Figure 4A** and **B**). This response became visible first at the area that was treated by auxin (ROI1) by 8s and then extended along the root in a shootward direction (ROI2, ROI3, and ROI4) over 120s duration. This observation in Col-wt was well aligned with previous reports using various Ca^{2+} visualization tools [43,46,47].

However, strikingly, the Ca^{2+} increase upon auxin treatment was significantly supressed in *dnd1*. Only a weak increase of Ca^{2+} was observed at the ROI1. Interestingly, this defect was largely recovered in *rdd1 cngc2* **(Figure 4B). Thus,** the Ca^{2+} increase was severely impaired in *dnd1* at all ROIs, supporting our observation of the partial insensitivity to auxin in *dnd1*. Interestingly, this impairment was clearly rescued by the *rdd1* mutation, especially at ROI1 **(Figure 4C)**. Taken together, we found that *dnd1* shows alterations in auxin-induced Ca^{2+} increase, strongly indicating the involvement of CNGC2 in auxin-mediated Ca^{2+} signaling.

DISCUSSION

Changes in $[Ca^{2+}]_{cyt}$ levels are required to activate various physiological responses in plants [1]. However, as of now, the mechanisms by which these processes occur are largely unknown. Here, we propose that the Ca^{2+} channel activity of CNGC2 plays a crucial role in growth and development through its role in auxin signaling. In addition, in the last few years, CNGC2 has been implicated in the regulation of SAM size through the CLAVATA signaling cascade as well as Ca^{2+} homeostasis [23,28]. Together, these findings challenge the longstanding view that CNGC2 is primarily involved in pathogen defense.

Through genetic and physiological studies, plant CNGCs have been implicated in a wide variety of biological functions such as development and abiotic and biotic stress responses [8,11,33]. *dnd1* (*cngc2*) was the first CNGC mutant identified by an alteration of HR upon pathogen infection, and since then, it has been the most well-studied CNGC mutant [12,15,48]. To understand it's signaling pathway, we have isolated the first suppressor of *dnd1, rdd1-1.* In this study, the causative mutation of *rdd1-1* was found to be a point mutation in the auxin biosynthesis gene *YUC6* consistent with leading to a loss-of-function allele.

Our results strongly suggest that CNGC2 is involved in auxin signaling in addition to its role in plant immunity. Auxin has also been implicated in plant immunity mainly through its antagonistic effect against SA [49,50]. Indeed, not only immunity related phenotypes of *cngc2 (dnd1*) were suppressed by *rdd1-1* but also those of the similar mutant, *cngc4* (*hlm1*/*dnd2*) [15]. On the other hand, the *cpr22* autoimmune phenotype, caused by the CNGC11/12 gain-of-function mutation (constitutive activation of Ca^{2+} signal [3]) was not affected by *rdd1-1* [27,51]*.* Since *cpr22* exhibited a more straightforward, typical SA-mediated autoimmune phenotype, these data suggest that CNGC2/CNGC4 and CNGC11/12-mediate immune signal through distinct pathways and there is a unique aspect in CNGC2/CNGC4-mediated immunity. Thus, we hypothesized that CNGC2 either plays a role in auxin signaling primarily and affects immunity as a consequence of the auxin signaling defect, or that CNGC2 plays a role in multiple

physiological aspects independently. Here, we show that loss-of-function mutants of CNGC2 are indeed impaired in multiple levels of TIR1/AFB-dependent auxin signaling. Thus, *cngc2* plants expressing the YCNano-65 bioreporter for Ca^{2+} revealed that CNGC2 is required for auxin-induced Ca^{2+} influx in the root. This link to auxin correlated with reduced induction of the DR5::GUS reporter and the *IAA1* gene as well as impairment in auxin-dependent inhibition of root growth and gravitropism. All these phenotypes were fully or partially reverted by the *rdd1* mutation. Although the mechanisms behind of this rescue by the *rdd1* mutation is not clear yet, these data strongly indicate the involvement of CNGC2 in auxin signaling and we propose that the autoimmune phenotype and HR impairment of *dnd1/cngc2* is a secondary effect via alterations in auxin responses, challenging the long-standing notion that CNGC2 is an immunity related Ca^{2+} channel.

There is accumulating evidence indicating Ca^{2+} as a second messenger in auxin signaling and transport [43,44,46,52,53]. Auxin may induce changes in $[Ca^{2+}]_{cyt}$ levels [42] by a process independent of the well described TRANSPORT INHIBITOR RESPONSE 1 (TIR1)-based auxin perception system [43]. Auxin-related proteins, such as the early auxin-responsive genes Small auxin up RNAs (*SAUR*s), may also bind to Ca^{2+} sensors such as CaM in a Ca^{2+} dependent manner [54]. Gravitropism, a phenomenon that causes the bending of roots in response to a change in gravity vector, relies on the asymmetric accumulation of auxin and Ca^{2+} in the lower side of the root [35,43,55,56]. Furthermore, auxin regulates the alkalinization of the apoplast during gravitropism by modulating intracellular Ca^{2+} concentrations [43] and the localization of auxin and activity of auxin efflux carriers PINFORMED (PIN) [57] is regulated by PINOID (PID) kinase, through its association with Ca^{2+} binding proteins [53]. While the exact source of Ca^{2+} (apoplastic vs. organellar) in these auxin-based responses is unclear, extracellular Ca^{2+} from the apoplast is likely important [44]. CNGC2 localizes at the plasma membrane and has been reported to be involved in Ca^{2+} influx to the cytosol from the extracellular apoplastic Ca^{2+} pool [20,26,58]. Thus,

CNGC2 is a likely Ca^{2+} channel that mediates auxin signaling-related Ca^{2+} fluxes at plasma membrane.

Recently published work suggests that some other CNGCs are involved in auxin-induced Ca^{2+} signaling. Especially, the Ca^{2+} channel activity of Arabidopsis CNGC14 was found to be important in mediating the auxin-dependent gravitropic response and root hair auxin influx [46,52]. Since CNGCs were suggested to form heterotetrameric channels [26], it is plausible that CNGC2 and 14 may form a functional Ca^{2+} channel to induce auxin related responses. Indeed, we have tested the defect of gravitropic response of *cngc2* along with *cngc14* under our experimental conditions and found a similar degree of impairment for both mutants (data not shown). However, CNGC14 is a member of group III of the Arabidopsis CNGC family and it is only distantly related to CNGC2 [59]. The expression patterns of these two genes and knockout mutant phenotypes are also distinct, indicating their diverse function and non-redundancy. Furthermore, the role of CNGC14 seems rather limited to specific aspect/timing of auxin responses or action in specific tissues such as the root hair [52]. Indeed, CNGC14 knockout mutants do not show any drastic developmental defect like *cngc2* (*dnd1*). Thus, CNGC14 and CNGC2 likely have different biological functions and are probably not redundant even in auxin related responses. A detailed comparison of these two CNGCs in auxin related function will provide us significant insights into the diversification of biological function of this channel family.

In summary, the initial discovery of *dnd1*, the *CNGC2* null mutant, which exhibits autoimmune phenotypes, implicated CNGC2 as a Ca^{2+} conducting channel involved in plant immunity [14,15]. However, publications in recent years and our current work strongly indicate its function beyond immunity. Thus, understanding the CNGC2 mediated signal transduction will provide us significant information of crosstalk between immunity and auxin (development) signaling via Ca^{2+} signals.

MATERIALS AND METHODS

Plant Materials and Growth Conditions. For phenotypic analyses, *A. thaliana* seeds were cold stratified at 4°C for 2 days prior to being grown at 23 °C on Sunshine-Mix #1™ (Sun Gro Horticulture Canada. Plants for the mapping populations were grown in a growth chamber with a 9-hour photoperiod (9 hour light/ 15 hour dark) and a day/night temperature regime of 22ºC/18ºC. For most experiments, plants were grown on petri dishes with ½ Murashige and Skoog (MS), 1% sucrose, and 0.8% (w/v) agar at pH 5.8 under ambient light conditions. Media was either supplemented with IAA of desired concentration or equal volumes of ethanol after autoclaving. Homozygous mutants were identified by PCR with primers listed in **Supplementary Table S4**.

Identification of *RDD1* as an allele of YUC6. Illumina® HiSeq 1500 system (Illumina, Inc., San Diego, CA, USA) at the McMaster Institute for Molecular Biology and Biotechnology (MOBIX) was used to sequence genomic DNA extracted from 4-week old leaves of *rdd1-1 cngc2-3* and *cngc2-3* plants. DNA was extracted from 100 mg of powdered leaf tissue using the CTAB method [60] with slight modification: To the CTAB extraction buffer was added 200 units/ml of RNAse A and 0.4 g/ml PVP (MW 40000) (Sigma-Aldrich Canada). Extracted DNA was precipitated twice with isopropanol, once with 75% EtOH and resuspended in 0.1X TE buffer supplemented with 0.2 units of RNAse A. DNA integrity was assessed using agarose gel electrophoresis and quantitated with a Quant-iT PicoGreen dsDNA Assay Kit (Thermo Fisher Scientific) on a Bio-Tek Powerwave HT microplate reader. Multiplex library preparation followed manufacturer's instructions (Nextera) and the three libraries were sequenced on one flow-cell lane in high throughput mode. Raw sequence reads were trimmed for adaptor sequences with

Cutadapt software [61] and unpaired reads, as well as those of length < 36 nt, were excluded from all further analyses. Paired reads were aligned against the TAIR10 Col-0 reference genome using BWA [62] and sequence variants were detected with the mpileup function of SAMtools [63].

GUS enzymatic assay. Seedlings were grown on ½ MS, 1% sucrose, and 0.8% (w/v) agar plates for 6 days before being transferred to plates supplemented with 1 μM IAA, or solvent alone, for 24 hours. GUS reporter activity was analyzed at excitation of 365 nm and emission of 455 nm using a TECAN plate reader (every 10 min for 2 hours) in the presence of 4-methylumbelliferyl glucuronide (4-MUG). GUS activity was standardized against protein concentration and data was reported as GUS activity in pmol 4-methylumbelliferone (4MU) per μg protein).

Pathogen infection. Infection with *Hyaloperonospora arabidopsidis* isolate Noco, which is virulent to Columbia ecotype of Arabidopsis was performed as described previously with 5 x 10^5 spores per ml [26].

Root growth inhibition. Sensitivity to auxin was analyzed as previously described by [38]. Seedlings were grown on minimal medium of ½ MS, 1% sucrose, and 0.8% agar supplemented with various concentrations of IAA. To analyze the root growth inhibition, the data of root growth on auxin media and minimal media was plotted.

Analysis of endogenous Salicylic acid. Endogenous SA was analyzed using the *Acinetobacter* sp. ADPWH lux-based biosensor as described [64].

Gravitropic root bending. Images of 5-7 day old seedlings were manually taken every 2 hours from 4 hours to 10 hours and then again at 24 hours after gravistimulation. The deviation in root tip angle from 90° was analyzed using the angle tool on ImageJ software (http://rsbweb.nih.gov/ij/).

DII:VENUS analysis For DII:VENUS analysis, seedlings were supplemented with 1µM IAA and visualized immediately for 20 minutes. Confocal images were taken using a Leica TCS SP5 confocal system with the acousto-optical beam splitter (HCX PL APO CS 40x immersion oil objective; numerical aperture, 1.25) with the acousto-optic tunable filter for the argon laser set at 20%. The detection window was set to 525 to 600 nm for YFP (Leica Microsystems). 7-9 day old seedings staining with 1x propidium iodide at 40X magnification. Images were further processed using Leica Las AF lite software.

FRET-based Ca^{2+} analysis by YC-Nano65

Multiple lines of Col-wt, *dnd1* and *rdd1 dnd1* carrying YC-Nano65 were generated. These plants were grown on the surface of a vertical agar plate with ½ MS, 1% (w/v) sucrose and 0.5% gellan gum at pH 5.8 under ambient light conditions, and 10 µl of 1 µM IAA was applied to the root tip area. FRET (cpVenus) and CFP signals from YC-Nano65 were acquired with a motorized fluorescence stereo microscope (SMZ-25, Nikon) equipped with image splitting optics (W-VIEW GEMINI, Hamamatsu Photonics) and a sCMOS camera (ORCA-Flash4.0 V2, Hamamatsu Photonics) as previously described [65,66]. For high-resolution confocal Ca^{2+} analysis, the transgenic plants were grown vertically under a thin layer (approximately 2 mm) of the growth medium [½ MS, 1% (w/v) sucrose and 0.5% gellan gum at pH 5.8] on a cover glass (24 × 50

mm, Fisher Scientific) for 6 days at 23 °C. The tip of the root was exposed by removing a small window (approximately 500 µm × 500 µm) from the gel, and 10 µl of 1 µM IAA was applied to the root tip area through this window. FRET (cpVenus) and CFP signals from YC-Nano65 were acquired with a laser scanning confocal microscope (LSM780/Elyra; Newcomb Imaging Center, Department of Botany, University of Wisconsin, Madison) as previously described [45]. The cpVenus/CFP ratio was calculated with 6D imaging and Ratio & FRET plug-in modules and the kymograph data were produced along the entire root over time (NIS-Elements AR, Nikon).

Accession numbers

Sequence data from this article can be found in the GenBank/EMBL data libraries under the following accession numbers: DND1 (CNGC2), AT5G15410, YUC6, AT5G25620.

Acknowledgements:

We thank Dr. Catherine Chan for providing the Ws *cngc2* seeds. This work was supported by a discovery grant from National Science and Engineering Research Council (NSERC) to K.Y., Graduate students fellowship from NSERC to, S.C., and KAKENHI (17H05007, 18H05491) to M.T.

REFERENCES

1. Dodd, A. N., Kudla, J. & Sanders, D. The Language of Calcium Signaling. *Annu. Rev. Plant Biol.* **61,** 593–620 (2010).

2. Yuan, P., Jauregui, E., Du, L., Tanaka, K. & Poovaiah, B. W. ScienceDirect Calcium signatures and signaling events orchestrate plant – microbe interactions. *Curr. Opin. Plant Biol.* **38,** 173–183 (2017).

3. Moeder, W., Phan, V. & Yoshioka, K. Ca2+ to the rescue – Ca2+ channels and signaling in plant immunity. *Plant Sci.*

4. Edel, K. H., Marchadier, E., Brownlee, C., Kudla, J. & Hetherington, A. M. The Evolution of Calcium-Based Signalling in Plants. *Curr. Biol.* **27,** R667–R679 (2017).

5. DeFalco, T. A., Bender, K. W. & Snedden, W. A. Breaking the code: Ca2+ sensor in plant signaling. *Biochem. J.* **425,** 27–40 (2010).

6. Spalding, E. P. & Harper, J. F. The ins and outs of cellular Ca2+ transport. *Curr. Opin. Plant Biol.* **14,** 715–720 (2011).

7. Demidchik, V., Shabala, S., Isayenkov, S., Cuin, T. A. & Pottosin, I. Calcium transport across plant membranes□: mechanisms and functions. *N. Biotechnol.* 1–21 (2018). doi:10.1111/nph.15266

8. Dietrich, P., Anschütz, U., Kugler, A. & Becker, D. Physiology and biophysics of plant ligand-gated ion channels. *Plant Biol.* **12,** 80–93 (2010).

9. Jammes, F., Hu, H. C., Villiers, F., Bouten, R. & Kwak, J. M. Calcium-permeable channels in plant cells. *FEBS J.* **278,** 4262–4276 (2011).

10. Zelman, A. K. *et al.* Evolutionary and structural perspectives of plant cyclic nucleotide-gated cation channels. *Front Plant Sci* **3,** 1–13 (2012).

11. DeFalco, T. A., Moeder, W. & Yoshioka, K. Opening the Gates: Insights into Cyclic Nucleotide-Gated Channel-Mediated Signaling. *Trends Plant Sci.* **21,** 903–906 (2016).

12. Moeder, W., Urquhart, W., Ung, H. & Yoshioka, K. The role of cyclic nucleotide-gated ion

channels in plant immunity. *Mol. Plant* **4,** 442–452 (2011).

13. Moeder, W. & Yoshioka, K. CNGCs break through—A rice cyclic nucleotide-gated channel paves the way for pollen tube growth. *PLoS Genet.* **13,** 1–5 (2017).
14. Clough, S. J. *et al.* The Arabidopsis dnd1 'defense, no death' gene encodes a mutated cyclic nucleotide-gated ion channel. *Proc. Natl. Acad. Sci. U. S. A.* **97,** 9323–9328 (2000).
15. Yu, I. C., Parker, J. & Bent, A. F. Gene-for-gene disease resistance without the hypersensitive response in Arabidopsis dnd1 mutant. *Proc. Natl. Acad. Sci.* **95,** 7819–7824 (1998).
16. Balagué, C. *et al.* HLM1, an Essential Signaling Component in the Hypersensitive Response, Is a Member of the Cyclic Nucleotide–Gated Channel Ion Channel Family. *Plant Cell* **15,** 365–379 (2003).
17. Jurkowski, G. I. *et al.* Arabidopsis DND2, a second cyclic nucleotide-gated ion channel gene for which mutation causes the 'defense, no death' phenotype. *Mol Plant Microbe Interact* **17,** 511–520 (2004).
18. Yoshioka, K. *et al.* The Chimeric Arabidopsis CYCLIC NUCLEOTIDE-GATED ION CHANNEL11/12 Activates Multiple Pathogen Resistance Responses. *Plant Cell* **18,** 747–763 (2006).
19. Urquhart, W. *et al.* The chimeric cyclic nucleotide-gated ion channel ATCNGC11/12 constitutively induces programmed cell death in a Ca2+ dependent manner. *Plant Mol. Biol.* **65,** 747–761 (2007).
20. Ali, R. *et al.* Death don't have no mercy and neither does calcium: Arabidopsis CYCLIC NUCLEOTIDE GATED CHANNEL2 and innate immunity. *Plant Cell* **19,** 1081–95 (2007).
21. Chan, C. W. M., Schorrak, L. M., Smith, R. K., Bent, A. F. & Sussman, M. R. A Cyclic Nucleotide-Gated Ion Channel, CNGC2,Is Crucial for Plant Development and Adaptation to Calcium Stress. *Plant Physiol.* **132,** 728–731 (2003).
22. Chan, C. W. M., Wohlbach, D. J., Rodesch, M. J. & Sussman, M. R. Transcriptional

changes in response to growth of Arabidopsis in high external calcium. *FEBS Lett.* **582,** 967–976 (2008).

23. Wang, Y. *et al.* CNGC2 Is a Ca2+ Influx Channel That Prevents Accumulation of Apoplastic Ca2+ in the Leaf. *Plant Physiol.* **173,** 1342–1354 (2017).
24. Katano, K., Kataoka, R., Fujii, M. & Suzuki, N. Differences between seedlings and flowers in anti-ROS based heat responses of Arabidopsis plants deficient in cyclic nucleotide gated channel 2. *Plant Physiol. Biochem.* **123,** 288–296 (2018).
25. Finka, A., Cuendet, A. F., Maathuis, F. J., Saidi, Y. & Goloubinoff, P. Plasma membrane cyclic nucleotide gated calcium channels control land plant thermal sensing and acquired thermotolerance. *Plant Cell* **24,** 3333–3348 (2012).
26. Chin, K., DeFalco, T. A., Moeder, W. & Yoshioka, K. The Arabidopsis cyclic nucleotide-gated ion channels AtCNGC2 and AtCNGC4 work in the same signaling pathway to regulate pathogen defense and floral transition. *Plant Physiol.* **163,** 611–24 (2013).
27. Fortuna, A. *et al.* Crossroads of stress responses, development and flowering regulation—the multiple roles of cyclic nucleotide gated ion channel 2. *Plant Signal. Behav.* **10,** 23–26 (2015).
28. Chou, H., Zhu, Y., Ma, Y. & Berkowitz, G. A. The CLAVATA signaling pathway mediating stem cell fate in shoot meristems requires Ca2+ as a secondary cytosolic messenger. *Plant J.* **85,** 494–506 (2016).
29. Mashiguchi, K. *et al.* The main auxin biosynthesis pathway in Arabidopsis. *Proc. Natl. Acad. Sci.* **108,** 18512–18517 (2011).
30. Won, C. *et al.* Conversion of tryptophan to indole-3-acetic acid by TRYPTOPHAN AMINOTRANSFERASES OF ARABIDOPSIS and YUCCAs in Arabidopsis. **108,** 18518–18523 (2011).
31. Kim, J. I. *et al.* yucca6, a Dominant Mutation in Arabidopsis, Affects Auxin Accumulation and Auxin-Related Phenotypes. *Plant Physiol.* **145,** 722–735 (2007).

32. Cheng, Y., Dai, X. & Zhao, Y. Auxin biosynthesis by the YUCCA flavin monooxygenases controls the formation of floral organs and vascular tissues in Arabidopsis. *Genes Dev.* **20,** 1790–1799 (2006).

33. Moeder, W., Urquhart, W., Ung, H. & Yoshioka, K. The role of cyclic nucleotide-gated ion channels in plant immunity. *Mol. Plant* **4,** 442–452 (2011).

34. Tanaka, H., Dhonukshe, P., Brewer, P. B. & Friml, J. Spatiotemporal asymmetric auxin distribution: A means to coordinate plant development. *Cell. Mol. Life Sci.* **63,** 2738–2754 (2006).

35. Sato, E. M., Hijazi, H., Bennett, M. J., Vissenberg, K. & Swarup, R. New insights into root gravitropic signalling. *J. Exp. Bot.* **66,** 2155–2165 (2015).

36. Fendrych, M. *et al.* Rapid and reversible root growth inhibition by TIR1 auxin signalling. *Nat Plants* **4,** 453–459 (2018).

37. Thimann, K. V. Auxins and the Inhibition of Plant Growth. *Biol. Rev.* **14,** 314–337 (1938).

38. Wilson, A. K., Pickett, F. B., Turner, J. C. & Estelle, M. A dominant mutation in Arabidopsis confers resistance to auxin, ethylene and abscisic acid. *MGG Mol. Gen. Genet.* **222,** 377–383 (1990).

39. Ulmasov, T., Murfett, J., Hagen, G. & Guilfoyle, T. J. Aux/IAA proteins repress expression of reporter genes containing natural and highly active synthetic auxin response elements. *Plant Cell* **9,** 1963–1971 (1997).

40. Brunoud, G. *et al.* A novel sensor to map auxin response and distribution at high spatio-temporal resolution. *Nature* **482,** 103–106 (2012).

41. Dela, R. K. & Leopold, A. C. A Role for Calcium in Auxin Transport. *Plant Physiol* **51,** 845–847 (1973).

42. Shishova, M. & Lindberg, S. Auxin induces an increase of Ca2+ concentration in the cytosol of wheat leaf protoplasts. *J. Plant Physiol.* **161,** 937–945 (2004).

43. Monshausen, G. B., Miller, N. D., Murphy, A. S. & Gilroy, S. Dynamics of auxin-

dependent Ca2+ and pH signaling in root growth revealed by integrating high-resolution imaging with automated computer vision-based analysis. *Plant J.* **65,** 309–318 (2011).

44. Vanneste, S. & Friml, J. Calcium- The Missing Link in Auxin Action. *Plants* **2,** 650–675 (2013).

45. Choi, W.-G., Toyota, M., Kim, S.-H., Hilleary, R. & Gilroy, S. Salt stress-induced Ca2+ waves are associated with rapid, long-distance root-to-shoot signaling in plants. *Proc. Natl. Acad. Sci.* **111,** 6497–6502 (2014).

46. Shih, H. W., Depew, C. L., Miller, N. D. & Monshausen, G. B. The cyclic nucleotide-gated channel CNGC14 regulates root gravitropism in Arabidopsis thaliana. *Curr. Biol.* **25,** 3119–3125 (2015).

47. Waadt, R., Krebs, M., Kudla, J. & Schumacher, K. Multiparameter imaging of calcium and abscisic acid and high-resolution quantitative calcium measurements using R-GECO1-mTurquoise in Arabidopsis. *New Phytol.* **216,** 303–320 (2017).

48. Wang, Y. *et al.* CNGC2 is a Ca2+ Influx Channel That Prevents Accumulation of Apoplastic Ca2+ in the Leaf. *Plant Physiol.* **173,** 1342–1354 (2017).

49. Koornneef, A. & Pieterse, C. M. J. Cross Talk in Defense Signaling. *Plant Physiol.* **146,** 839–844 (2008).

50. Mutka, A. M., Fawley, S., Tsao, T. & Kunkel, B. N. Auxin promotes susceptibility to Pseudomonas syringae via a mechanism independent of suppression of salicylic acid-mediated defenses. *Plant J.* **74,** 746–754 (2013).

51. Fortuna, A. Investigating the interplay of Cyclic Nucleotide Gated Ion Channel 2 and auxin in immune signaling. (University of Toronto, 2015).

52. Dindas, J. *et al.* AUX1-mediated root hair auxin influx governs SCFTIR1/AFB-type Ca2+ signaling. *Nat. Commun.* **9,** (2018).

53. Benjamins, R., Ampudia, C. S. G., Hooykaas, P. J. J. & Offringa, R. PINOID-Mediated Signaling Involves Calcium-Binding Proteins. *Plant Physiol.* **132,** 1623–1630

54. Yang, T. & Poovaiah, B. W. Molecular and Biochemical Evidence for the Involvement of Calcium Calmodulin in Auxin Action. *J. Biol. Chem.* **275,** 3137–3143 (2000).

55. Bennett, M. J. *et al.* Arabidopsis AUX1 gene: a permease-like regulator of root gravitropism. *Science (80-.).* **273,** 948–950 (1996).

56. Wang, R. *et al.* HSP90 regulates temperature-dependent seedling growth in Arabidopsis by stabilizing the auxin co-receptor F-box protein TIR1. *Nat. Commun.* **7,** 1–10 (2016).

57. Kleine-Vehn, J. *et al.* Gravity-induced PIN transcytosis for polarization of auxin fluxes in gravity-sensing root cells. *Proc. Natl. Acad. Sci.* **107,** 22344–22349 (2010).

58. Lemtiri-chlieh, F. & Berkowitz, G. A. Cyclic Adenosine Monophosphate Regulates Calcium Channels in the Plasma Membrane of Arabidopsis Leaf Guard and Mesophyll Cells. *J. Biol. Chem.* **279,** 35306–35312 (2004).

59. Maser, P. *et al.* Phylogenetic Relationships within Cation Transporter Families of Arabidopsis. *Plant Physiol.* **126,** 1646–1667 (2001).

60. Thompson, W. F. Rapid isolation of higher weight plant DNA. *Nucleic Acids Res.* **8,** 4321–4325 (1980).

61. Martin, M. Cutadapt removed adapter sequences from high-throughput sequencing read. *EMBnet.journal* **17,** 5–7 (2011).

62. Li, H. & Durbin, R. Fast and accurate short read alignment with Burrows – Wheeler transform. **25,** 1754–1760 (2009).

63. Li, H. *et al.* The Sequence Alignment / Map format and SAMtools. **25,** 2078–2079 (2009).

64. Defraia, C. T., Schmelz, E. A. & Mou, Z. A rapid biosensor-based method for quantification of free and glucose-conjugated salicylic acid. *Plant Methods* **4,** 1–11 (2008).

65. Toyota, M. *et al.* Glutamate triggers long-distance, calcium-based plant defense signaling. *Science (80-.).* **6,** 1112–1115 (2018).

66. Lenglet, A. *et al.* Control of basal jasmonate signalling and defence through modulation of

intracellular cation flux capacity. *New Phytol.* **216,** 1161–1169 (2017).

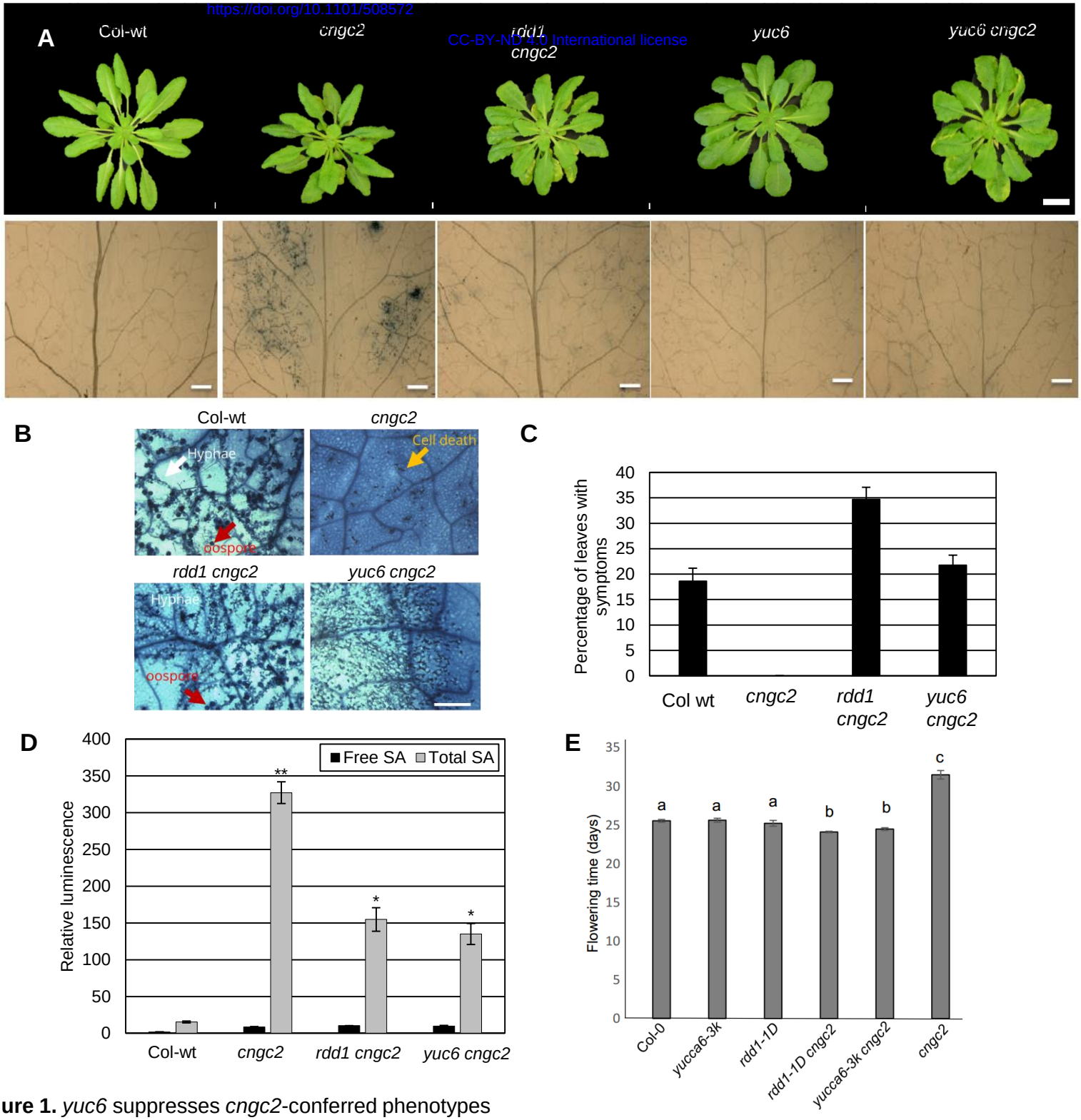

Figure 1. *yuc6* suppresses *cngc2*-conferred phenotypes

(A) (Top panel) Overall morphology of 5 week old Col-wt and mutant plants grown in short day conditions (9L:15D). *yuc6 cngc2* partially suppress *cngc2*-conferred dwarf morphology to the same degree as *rdd1 cngc2*. *yuc6*, the YUC6 knockout line, has shorter and wider rosette leaves compared to Col-wt. Scale bar = 1 cm. (Bottom panel) Corresponding trypan blue staining reveals a reduction in cell death in *yuc6 cngc2* compared to *cngc2*. Scale bar = 0.5 mm.

(B) Breakdown of hyper-resistance phenotype of *dnd1* in *rdd1 cngc2* and *yuc6 cngc2* double mutants upon infection with *H. arabidopsidis (Hpa)*, isolate Noco2. Trypan Blue staining of Col wild-type, and mutants were inoculated with *Hpa* isolate Noco2, at a suspension of 8 × 10^5 spores mL^{-1} and monitored for Bar = 1 mm

(C) Disease severity as a percentage of leaves showing symptoms of sporangiophore formation and leaf yellowing. *n* = 6.

(D) Salicylic acid (SA) levels (free SA + SA-glucoside) in 3- to 4-week-old wild-type and mutant leaves. SA levels are significantly different in *rdd1 cngc2* and *yuc6 cngc2* from *cngc2.* Shown are relative luminescence levels of *Acinetobacter* sp. ADPWH_lux. Error bars indicate SE of three replicates. Bars marked with asterisks indicate significant differences (Student's t test, P<0.05).

(E) *rdd1-1* and *yuc6* repress the delayed flowering phenotype of *cngc2*. *cngc2* plants exhibit delayed flowering compared to Col-wt, *rdd1-1 cngc2* and *yuc6 cngc2*. Error bars = averages SE. Bars marked with the same letter indicate no significant difference (Student's t-test, P < 0.05).

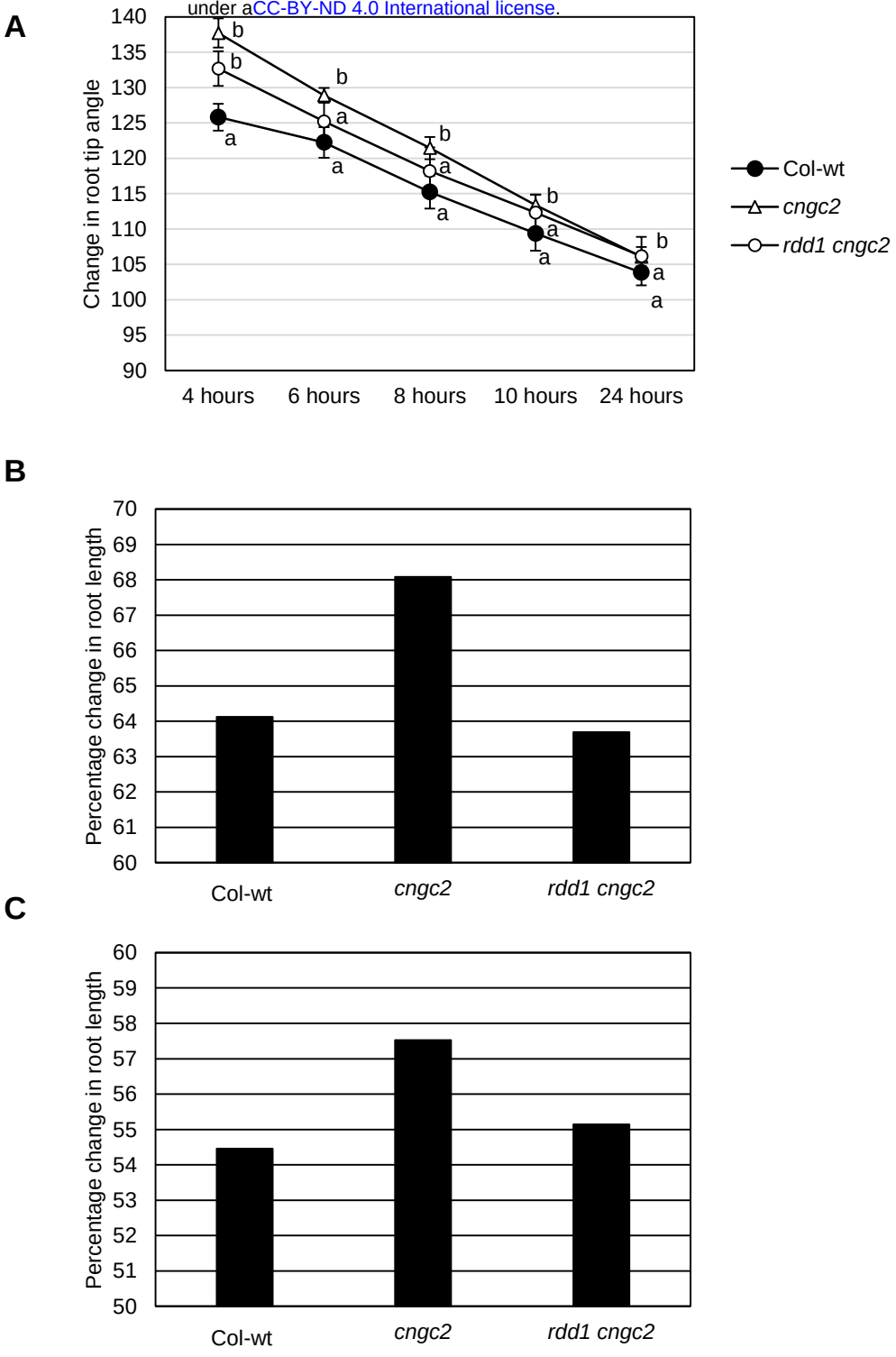

Figure 2. *dnd1* exhibits alterations in auxin-related phenotypes

(A)Time-course of gravitropic response of of 7 day old seedlings measured every 2 hours from 4 hours till 24 hours after rotating the plate by 90°. *cngc2* displays delayed gravitropic root bending and this is partially recovered in *rdd1 cngc2.* Shown are averages ± SE (n=70). Data points marked with the same letter indicate no significant difference (Student's t-test, $P < 0.05$).

(B) Percentage change in root length upon treatment with 0.1 µM IAA. *cngc2* is partially resistant to 0.1 µM IAA. Shown are averages ± SE (n=70)

(C) Percentage change in root upon treatment with 0.1 µM NAA. *cngc2* is partially resistant to 0.1 µM NAA. Shown are averages ± SE (n=70)

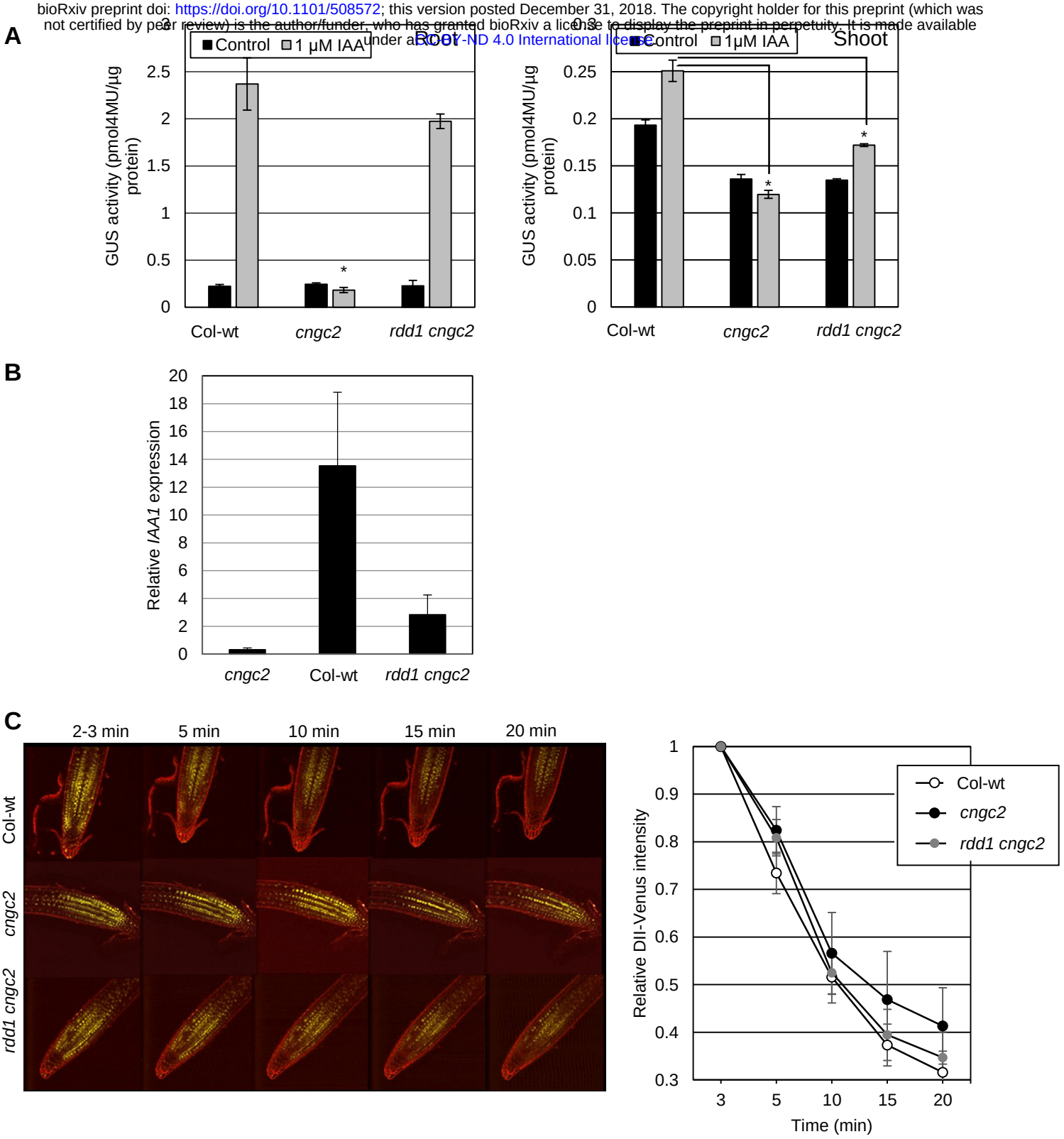

Figure 3. *cngc2* exhibits alterations in auxin-sensitivity which is partially rescued in *rdd1 cngc2*

(A) GUS activity of DR5::GUS transgenic plants (Col wt, *cngc2*, *rdd1 cngc2*). *cngc2* is insensitive to the application of 1µM exogenous IAA in its roots. This insensitivity is completely rescued in *rdd1 cngc2* roots (left). *cngc2* is also insensitive to the application of exogenous 1µM IAA in its shoots. This insensitivity is partially rescued in *rdd1 cngc2* shoots (right). Shown are averages ± SE, n = 3

(B)IAA1 transcript levels in 9 day old Col-wt, *cngc2* and *rdd1 cngc2* whole seedlings measured by qRT-PCR. IAA1 expression is shown relative to EF-1α. Shown are averages ± SE, n = 3. Bars marked with different letters indicate significant differences (Student's t test, $P < 0.05$).

(C)DII::VENUS fluorescence of the primary root after the addition of 1µM IAA. (Left) Shown are representative images. (Right) Quantification of signal intensity of DII::VENUS at region of interest (ROI), relative to two minutes after the addition of 1µM IAA. Degradation of VENUS signal is delayed in *cngc2* relative to Col-wt and *rdd1 cngc2*. Shown are ± SE, n = 5

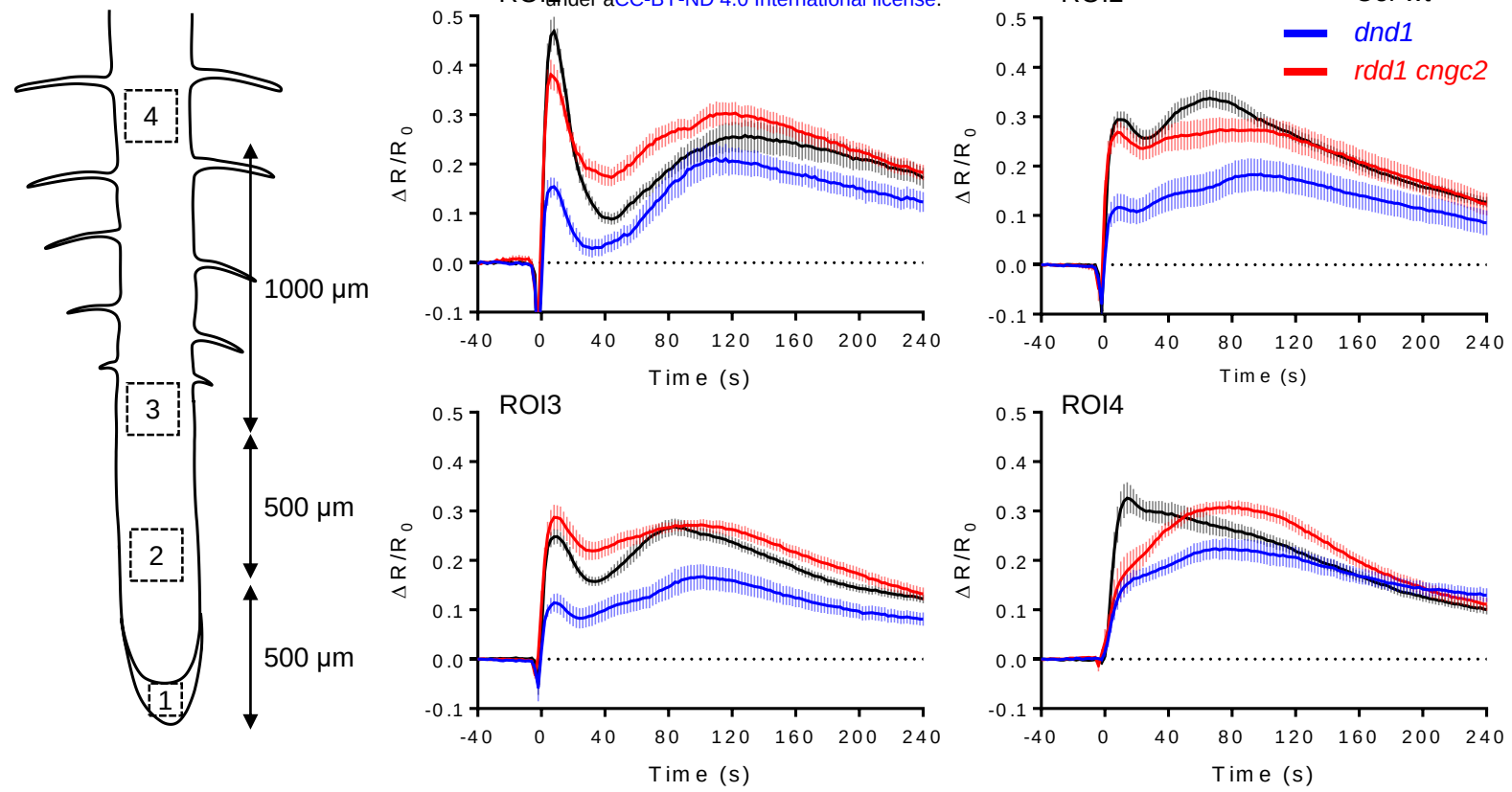

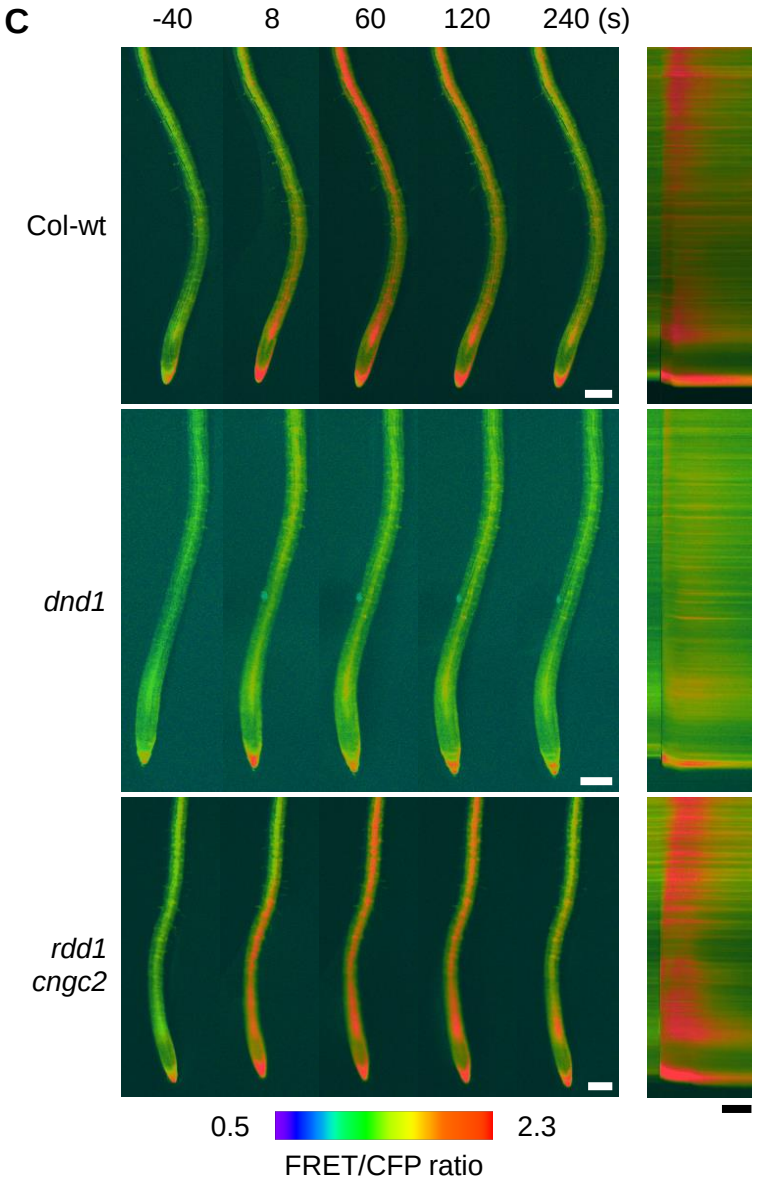

Figure 4. Auxin-mediated Ca^{2+} signaling is defective in *dnd1* but rescued in *rdd1 cngc2*.

(A) Schematic of region of interests (ROI) of the *A. thaliana* root that were examined for auxin-induced Ca^{2+} signaling. IAA (1 µM) was applied to the root tip region around ROI1.

(B) Quantitative analysis using the FRET based Ca^{2+} sensor YCNano-65. The application of 1µM IAA at 0 s induces Ca^{2+} spikes in columella cells (ROI1), elongation zone (ROI2 and ROI3) and the maturation zone (ROI4) of Col-wt root (n = 12) but not in these corresponding regions of *dnd1* (n = 10). This is largely recovered in *rdd1 cngc2* (n = 10).

(C) Kymograph analysis of changes in FRET/CFP ratio upon the addition of 1µM IAA in in Col-wt, *dnd1* and *rdd1 cngc2* background. White scale bar = 0.2 mm, black scale bar = 100 s.